NUWC-NPT TM 932042

NAVAL UNDERSEA WARFARE CENTER DIVISION
NEWPORT, RHODE ISLAND

Technical Memorandum

A FRACTIONAL-STEP TECHNIQUE FOR UNSTEADY INCOMPRESSIBLE FLOWS

Date: 31 March 1993

Prepared by: Stephen A. Jordan
Stephen A. Jordan
Launcher Systems
Development Division
Launcher and Missile
Systems Department

Approved for public release; distribution is unlimited.

Report Documentation Page

Form Approved
OMB No. 0704-0188

1. REPORT DATE	2. REPORT TYPE	3. DATES COVERED
31 MAR 1993	**Technical Memo**	**31-03-1993 to 31-03-1993**

4. TITLE AND SUBTITLE
A Fractional-Step Technique for Unsteady Incompressible Flows

5a. CONTRACT NUMBER

5b. GRANT NUMBER

5c. PROGRAM ELEMENT NUMBER

6. AUTHOR(S)
Stephen Jordan

5d. PROJECT NUMBER
AL0118

5e. TASK NUMBER

5f. WORK UNIT NUMBER

7. PERFORMING ORGANIZATION NAME(S) AND ADDRESS(ES)
Naval Undersea Warfare Center Division,1176 Howell Street,Newport,RI,02841

8. PERFORMING ORGANIZATION REPORT NUMBER
TM 932042

9. SPONSORING/MONITORING AGENCY NAME(S) AND ADDRESS(ES)

10. SPONSOR/MONITOR'S ACRONYM(S)

11. SPONSOR/MONITOR'S REPORT NUMBER(S)

12. DISTRIBUTION/AVAILABILITY STATEMENT
Approved for public release; distribution unlimited

13. SUPPLEMENTARY NOTES
NUWC2015

14. ABSTRACT
A numerical technique is presented for efficiently solving three-dimensional unsteady incompressible flows. The method is based on the fractional-step approach. The computational molecule is a semi-staggered grid where the velocity components are defined at the cell corners and the pressure at the cell centers. The pressure gradients at the cell interfaces are computed using fourth-order-accurate compact differences. The convective terms are time-advanced by a third-order-accurate Runge-Kutta technique and the diffusive terms by the Crank-Nicolson scheme. The residual form of the pressure-Poisson equation is solved iteratively by the modified strongly implicit scheme. Globally, the method is second-order accurate in space and time. The consistency of the boundary conditions and the overall solution accuracy are verified properly. The technique is applied to a three-dimensional shear-driven cavity for predicting the unsteady flow at Reynolds numbers of 2000 and 3200.

15. SUBJECT TERMS
three-dimensional unsteady incompressible flows; Runge-Kutta; Crank-Nicolson; pressure-Poisson

16. SECURITY CLASSIFICATION OF:			17. LIMITATION OF ABSTRACT	18. NUMBER OF PAGES	19a. NAME OF RESPONSIBLE PERSON
a. REPORT	b. ABSTRACT	c. THIS PAGE			
unclassified	**unclassified**	**unclassified**	**Same as Report (SAR)**	**35**	

Report Documentation Page

Form Approved
OMB No. 0704-0188

1. REPORT DATE	2. REPORT TYPE	3. DATES COVERED
31 MAR 1993	**Technical Memo**	**31-03-1993 to 31-03-1993**

4. TITLE AND SUBTITLE
A Fractional-Step Technique for Unsteady Incompressible Flows

5a. CONTRACT NUMBER

5b. GRANT NUMBER

5c. PROGRAM ELEMENT NUMBER

6. AUTHOR(S)
Stephen Jordan

5d. PROJECT NUMBER
AL0118

5e. TASK NUMBER

5f. WORK UNIT NUMBER

7. PERFORMING ORGANIZATION NAME(S) AND ADDRESS(ES)
Naval Undersea Warfare Center Division,1176 Howell Street,Newport,RI,02841

8. PERFORMING ORGANIZATION REPORT NUMBER
TM 932042

9. SPONSORING/MONITORING AGENCY NAME(S) AND ADDRESS(ES)

10. SPONSOR/MONITOR'S ACRONYM(S)

11. SPONSOR/MONITOR'S REPORT NUMBER(S)

12. DISTRIBUTION/AVAILABILITY STATEMENT
Approved for public release; distribution unlimited

13. SUPPLEMENTARY NOTES
NUWC2015

14. ABSTRACT
A numerical technique is presented for efficiently solving three-dimensional unsteady incompressible flows. The method is based on the fractional-step approach. The computational molecule is a semi-staggered grid where the velocity components are defined at the cell corners and the pressure at the cell centers. The pressure gradients at the cell interfaces are computed using fourth-order-accurate compact differences. The convective terms are time-advanced by a third-order-accurate Runge-Kutta technique and the diffusive terms by the Crank-Nicolson scheme. The residual form of the pressure-Poisson equation is solved iteratively by the modified strongly implicit scheme. Globally, the method is second-order accurate in space and time. The consistency of the boundary conditions and the overall solution accuracy are verified properly. The technique is applied to a three-dimensional shear-driven cavity for predicting the unsteady flow at Reynolds numbers of 2000 and 3200.

15. SUBJECT TERMS
three-dimensional unsteady incompressible flows; Runge-Kutta; Crank-Nicolson; pressure-Poisson

16. SECURITY CLASSIFICATION OF:			17. LIMITATION OF ABSTRACT	18. NUMBER OF PAGES	19a. NAME OF RESPONSIBLE PERSON
a. REPORT	b. ABSTRACT	c. THIS PAGE			
unclassified	**unclassified**	**unclassified**	**Same as Report (SAR)**	**35**	

ABSTRACT

A numerical technique is presented for efficiently solving three-dimensional unsteady incompressible flows. The method is based on the fractional-step approach. The computational molecule is a semi-staggered grid where the velocity components are defined at the cell corners and the pressure at the cell centers. The pressure gradients at the cell interfaces are computed using fourth-order-accurate compact differences. The convective terms are time-advanced by a third-order-accurate Runge-Kutta technique and the diffusive terms by the Crank-Nicolson scheme. The residual form of the pressure-Poisson equation is solved iteratively by the modified strongly implicit scheme. Globally, the method is second-order accurate in space and time. The consistency of the boundary conditions and the overall solution accuracy are verified properly. The technique is applied to a three-dimensional shear-driven cavity for predicting the unsteady flow at Reynolds numbers of 2000 and 3200.

ADMINISTRATIVE INFORMATION

This memorandum was prepared under FY92/93 Project No. AL0118, principal investigator Stephen A. Jordan (Code 8322). This work was sponsored by ONR Scientific Officer Dr. L. P. Purtell, Code 1132F, and the NUWCDIVNPT Independent Research Program, Coordinator K. Lima, Code 102.

The author of this memorandum is located at the Naval Undersea Warfare Center Division, Newport, RI 02841-1708.

TABLE OF CONTENTS

LIST OF ILLUSTRATIONS

LIST OF ILLUSTRATIONS (Cont'd)

INTRODUCTION

Prediction methods of multi-dimensional, unsteady, incompressible flows can now investigate many engineering problems of practical importance. This is possible principally because of recent advancements in supercomputer technology. Besides the flow being unsteady, the problem geometry is often complicated. Airfoils, intakes, blade passages, heat exchangers, recessed cavities, and wall mounted bodies are just a few examples. In these problems, the numerical results can provide sufficient detail to gain a comprehensive understanding of the basic unsteady flow physics.

Basically, three distinct approaches are available for solving unsteady incompressible flows. One particular class of methods is founded on the fractional-step procedure (also called the projection method) proposed by Chorin [1] over twenty-five years ago. This procedure capitalizes on Helmholtz's decomposition theorem in which the convection and diffusion components of the unsteady Navier-Stokes equations are together decomposed into the sum of a divergence-free vector (velocity) and an irrotational vector (pressure gradient). Splitting the operators in this way permits the introduction of an intermediate velocity which provides the only direct link between the pressure and physical velocity fields. The Navier-Stokes equations are replaced by a two-step process which involves solution of an unsteady convection-diffusion equation for the intermediate velocity followed by an update of the physical velocity field. In the original two-dimensional scheme by Chorin, the method of artificial compressibility was implemented to establish a separate equation for solution of the pressure variable. Given the intermediate velocity field, the physical velocity and pressure fields were successively updated until the iterations converged. Convergence was defined by the allowable error in the incompressibility constraint. At each time increment, many iterations were necessary to minimize that error. Herein, a variation of Chorin's original fractional-step method is utilized. But before presenting the details of the technique, alternate methods that one can choose for solving unsteady incompressible flows are discussed.

Full predictor-corrector type schemes have also been applied to unsteady incompressible flows. One approach (referred to as a pressure-based method) involves replacing the continuity equation with a pressure-Poisson type equation which is derived by taking the divergence of the momentum equation and invoking the incompressibility constraint. The pressure-Poisson equation along with momentum are converged to each new time level by a semi-implicit prediction and correction sequence. Convergence is commonly achieved by minimizing the residual (or error) of the discretized pressure-Poisson equation. For steady flows, large time steps are allowed to accelerate convergence to steady-state. The most recent release of this approach is called PISO (Pressure-Implicit with Splitting of Operators) [2]. Its roots lie in the SIMPLE (Semi-Implicit Method for Pressure-Linked Equations) algorithm [3]. In PISO, the

predictor-corrector steps arise from a splitting of operators in the discretized momentum and pressure-Poisson equations. For the steady flow problem, SIMPLE iterates to steady-state convergence while PISO advances in time. Thus, PISO is equally applicable to unsteady and transient flows. Due to the explicit definitions in the corrector steps however, under-relaxation may be necessary in PISO to sustain convergence during the predictor-corrector solution sequence [4].

The third basic approach for predicting unsteady incompressible flows is the "method of pseudo-compressibility" [5]. This method was introduced by Chorin [6] for computing steady incompressible flows. Chorin's idea resolved the difficulty of having an explicit definition for the pressure variable in the incompressible flow equations. He proposed to couple the continuity and momentum equations by adding a pressure-like time-dependent term to the continuity equation. This term physically represents the imposition of finite-speed pressure waves onto the incompressible velocity field. The pressure waves are time-advanced (along with momentum) until they theoretically vanish. At convergence the incompressibility constraint is satisfied, and the pressure field is now fully known. For the steady flow problem, it is important to note that the advancement of the velocity and pressure fields to steady-state is accomplished strictly through pseudo time. Consequently, the intermediate solutions are not time accurate. Recently however, the method of pseudo-compressibility was extended to unsteady incompressible flows (see Soh and Goodrich [7] or Rogers and Kwak [8]). The new system of equations is essentially the same as the original set except for a second time-dependent velocity term in the momentum equation. While the original time-dependent term represents real time, the second term allows for marching in pseudo time. Thus, pseudo steady-state convergence is achieved for each physical time increment. When using this approach, one should be concerned about the local error tolerance associated with pseudo steady-state convergence relative to the leading temporal truncation error of the physical system.

Presented here is a solution technique for solving unsteady incompressible flows that is based on the original fractional-step method developed by Chorin along with the variations proposed by Kim and Moin [9] and Rai and Moin [10]. The present technique differs from those previous works in three basic aspects. First, the grid is semi-staggered, meaning that the pressure is computed at the grid cell centers while the velocity components are collocated with the grid points. Construction of the computational molecule in this fashion greatly facilitates derivation of a consistent set of boundary conditions for the intermediate velocity. Second, strong coupling is maintained between the pressure and velocity components through introduction of a fourth-order-accurate compact differencing scheme for computing the pressure gradients. Lastly, the modified strongly implicit procedure is implemented for solution of the residual form of the discretized pressure-Poisson equation in three dimensions. For the moment, the temporal and spatial discretization of the

governing equations, implementation of the solution algorithms and test cases are presented in Cartesian coordinates. The numerical accuracy of the solution technique and the consistency of the boundary conditions are verified by simulating an exact solution of the two-dimensional Navier-Stokes equations. The technique is then used to predict the flow in a three-dimensional shear-driven cavity at Reynolds numbers of 2000 and 3200. At these Reynolds numbers the flow is unsteady and strictly laminar. The test cases include comparisons between the numerical results and published experimental data.

FORMULATION AND DISCRETIZATION

The mathematical system which governs unsteady incompressible flows is the Navier-Stokes (NS) equations with continuity. In index notation, the conservative non-dimensional form of this primitive-variable system in three-dimensional (3D) Cartesian coordinates is

$$\frac{\partial u_i}{\partial t} + \frac{\partial u_i u_j}{\partial x_j} = -\frac{\partial p}{\partial x_i} + \frac{1}{Re}\frac{\partial^2 u_i}{\partial x_j \partial x_j}, \tag{1a}$$

$$\frac{\partial u_i}{\partial x_i} = 0, \tag{1b}$$

where the velocity vector $u_i = < u,v,w >^T$ and p is the pressure. The Reynolds number $Re = UL/\nu$; ν is the kinematic viscosity and U and L are the reference velocity and length, respectively.

Here, Chorin's original fractional-step method along with the variations proposed by Kim and Moin [9] and Rai and Moin [10] are combined to temporally discretize the system in equation (1). Kim and Moin time-split the convective and diffusive terms in the momentum equation using an explicit second-order-accurate Adams-Bashforth method and an implicit Crank-Nicolson scheme, respectively. Use of the Crank-Nicolson scheme eliminates the viscous stability restriction which can be severe near the wall even in high-Re flows. As pointed out by Rai and Moin however, the Adams-Bashforth method is unconditionally unstable when applied to the linear convection equation. In their solution technique, they chose to time-split the convective terms using a third-order-accurate Runge-Kutta procedure. The procedure was subsequently improved by Le and Moin [11] in terms of a reduced computational requirement by solving the pressure-Poisson equation only in the final step of the Runge-Kutta procedure. For the linear convection equation, this particular procedure is conditionally stable. Contrasting the numerical stability of the Adams-Bashforth method and Runge-Kutta procedure is presented later in the Numerical Stability section.

The Runge-Kutta/Crank-Nicolson solution sequence adopted here for time-advancement of the system of equations in (1) involves three complete

steps to update the physical velocity components and pressure variable. This sequence has the form

$$\frac{\hat{u}_i^m - u_i^{n,m-1}}{\Delta t} = -\alpha^m \left(u_j \frac{\partial u_i}{\partial x_j} \right)^{n,m-1} - \beta^m \left(u_j \frac{\partial u_i}{\partial x_j} \right)^{n,m-2} + \frac{\gamma^m}{Re} \frac{\partial^2 \left(\hat{u}_i^m + u_i^{n,m-1} \right)}{\partial x_j \partial x_j}, \quad (2a)$$

$$\frac{u_i^{n,m} - \hat{u}_i^m}{\Delta t} = -\frac{1}{\Delta t} \frac{\partial \Phi^m}{\partial x_i}, \quad (2b)$$

$$\frac{\partial u_i^{n,m}}{\partial x_i} = 0, \quad (2c)$$

$$\frac{\partial^2 \Phi^m}{\partial x_i \partial x_i} = \frac{1}{\Delta t} \frac{\partial \hat{u}_i^m}{\partial x_i}, \quad (2d)$$

$$\Phi^m = \alpha^m \phi^m + \beta^m \phi^{m-1}, \quad (2e)$$

$$p = \phi + \frac{\Delta t}{2\,Re} \frac{\partial^2 \phi}{\partial x_i \partial x_i}, \quad (2f)$$

where $\alpha = \left\langle \frac{8}{15}, \frac{5}{12}, \frac{3}{4} \right\rangle$, $\beta = \left\langle 0, -\frac{17}{60}, \frac{5}{12} \right\rangle$, and $\gamma = \left\langle \frac{4}{15}, \frac{1}{15}, \frac{1}{6} \right\rangle$.

The parameter n denotes the particular time level and m signifies the three steps of the Runge-Kutta procedure; the velocities $u_i^{n,-1} = 0$, $u_i^{n,0} = u_i^n$ and $u_i^{n,3} = u_i^{n+1}$. A pressure variable ϕ replaces the actual pressure p in the velocity update equation due to the implicit treatment of the diffusion term. An exact relationship between ϕ and p is given by the simple expression in (2f). As in the pressure-based method, a Poisson type equation is derived for solution of the pressure variable ϕ by taking the divergence of the velocity update equation in (2b) and enforcing continuity [equation (2c)]. The result shown in equation (2d) provides for the solution of ϕ in terms of the divergence of the intermediate velocity field $\hat{u}_i$. This velocity field does not satisfy incompressibility because the pressure gradient is eliminated from the momentum equation. Since the intermediate velocity and pressure-Poisson equations are solved independently, it is not necessary to treat the Runge-Kutta coefficients explicitly for updating the physical velocity field. A second scalar field Φ is therefore introduced of which the pressure can be computed exactly anytime during the computation through expressions (2e) and (2f). It should be noted that by retaining the Crank-Nicolson scheme for the diffusive terms, the solution accuracy of this fractional-step technique is second order in time.

One should notice that the system of equations in (2) is now in a nonconservative form. This form facilitates implementation of local high-order spatial accuracy for the convective terms. Inasmuch as flow discontinuities are absent from the applications considered here, the nonconservative form should give results comparable to that of the conservative form [10]. Except for the convective terms, all spatial derivatives shown in the Runge-Kutta/Crank Nicolson solution sequence are discretized by second-order central differences. The convective terms are explicit and are spatially discretized by a third-order-accurate five-point upwind-biased stencil. Velocity points which reside outside the grid boundaries in the stencil are determined by extrapolating the field results to the second order [12]. This spatial discretization and extrapolation scheme leads to numerical solutions which are globally second-order accurate in space.

SOLUTION METHODOLOGY

In this section, specific details are presented about the procedures used for solving the intermediate velocity equation independent of the pressure-Poisson equation. Establishing proper coupling between the velocity components and pressure variable is an essential ingredient of the method to inhibit spurious oscillations. As illustrated in detail by Patankar [13], fully staggered grids satisfy this demand ideally, but require extrapolation or reflection of the field results for assigning values to the point velocities which lie outside the geometric boundaries. The extrapolation becomes particularly cumbersome for spatial differencing approximations that are higher than second order. One can also implement a semi-staggered pattern in which the velocity components are positioned at the grid points and the pressures are located at the grid cell centers. Besides having the velocity field now defined directly on the boundary, this grid also offers the advantage of deriving a consistent set of boundary conditions for the intermediate velocity. Without proper care in the discretization definitions, solution difficulties with this choice will arise because the grid cell pressures can actually become uncoupled from their adjacent neighbors [14]. Described below is a computational molecule and solution procedure that exploits the advantages of the semi-staggered grid pattern while maintaining strong coupling between the velocity components and pressure variable.

The two-dimensional (2D) computational molecule in Figure 1 shows the relative positions of the velocity components and the pressure variable on the grid. The velocity components are collocated with the grid points, but the pressure variable is staggered. The source term in the pressure-Poisson equation is computed by averaging the grid cell corner velocities. If the pressure gradient in the velocity update equation is now determined by averaging the pressures at the grid cell centers, then the semi-staggered grid which uncouples the cell pressures from their adjacent neighbors will be recovered. To avert this dilemma, the pressure gradients are first computed at the cell interfaces (indicated by the arrows in Figure 1) by a

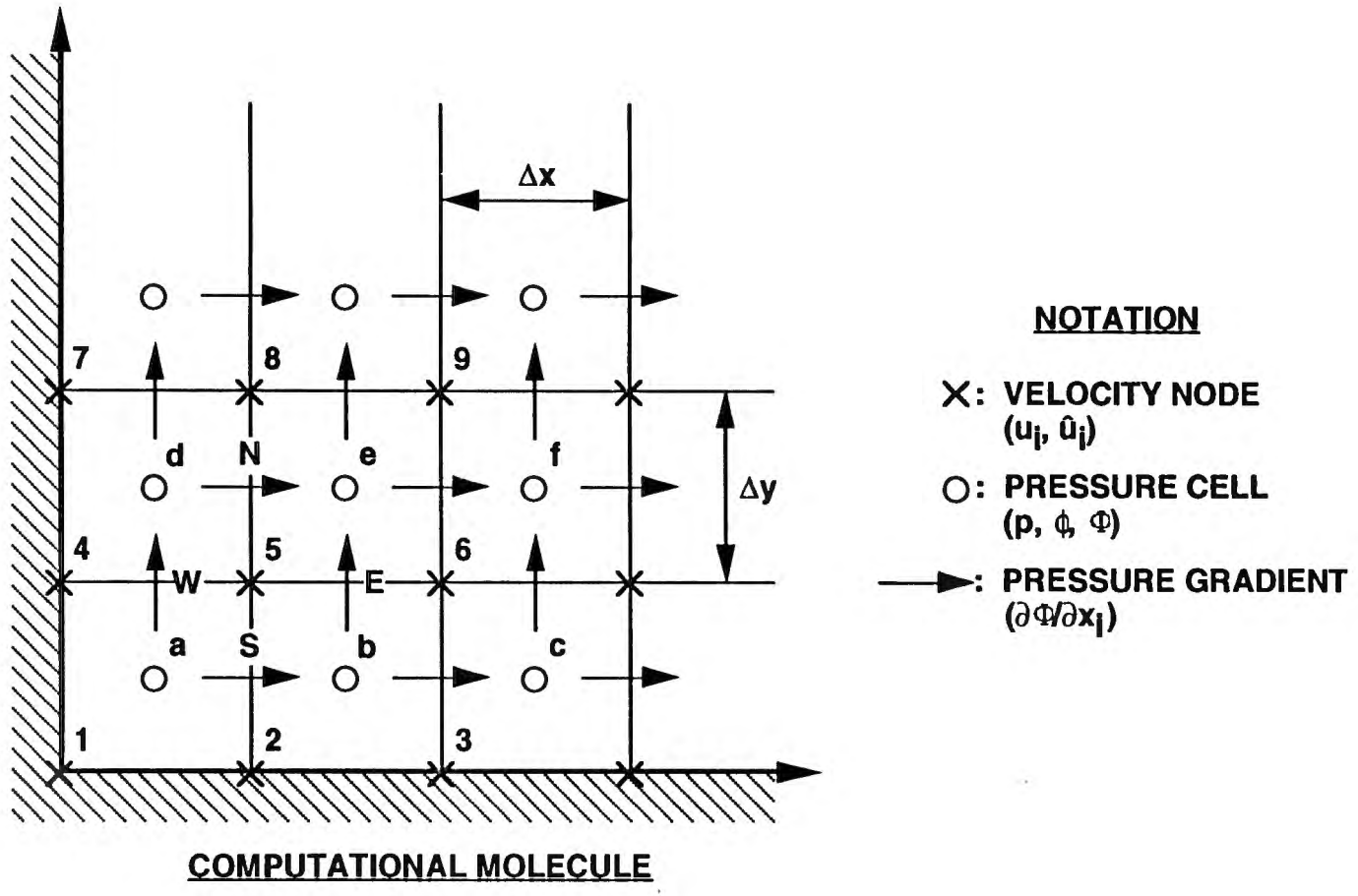

COMPUTATIONAL MOLECULE

Figure 1. Computational Molecule Used for Discretizing the Incompressible Navier-Stokes Equations

fourth-order-accurate compact differencing formula. The pressure gradients needed to update the point velocities are obtained by averaging the appropriate values at the cell interfaces. For example, the u-velocity at point 5 is updated by averaging the pressure gradients at cell interfaces marked N and S. Likewise, the pressure gradients at the W and E cell interfaces are averaged together to update the corresponding v-velocity. By computing the pressure gradients in this manner, the velocity components and pressure variable remain strongly coupled. Also, no superfluous errors are introduced because the accuracy of the pressure gradients are within the leading truncation error of the overall solution technique.

After solving the pressure Poisson equation for Φ^m, the pressure gradient is computed by the fourth-order-accurate compact scheme. For example, at the cell interface labeled S in Figure 1,

$$f_{i+1} + 22f_i + f_{i-1} = \frac{24\left(\Phi^m_{i+½} - \Phi^m_{i-½}\right)}{\Delta x}, \tag{3}$$

where $f_i = (\partial \Phi^m / \partial x)_i$. The index i symbolizes the center point at cell interface S and i + 1/2 denotes the cell center marked (b). Likewise, at cell interface W

$$g_{j+1} + 22g_j + g_{j-1} = \frac{24\left(\Phi^m_{j+½} - \Phi^m_{j-½}\right)}{\Delta y}, \tag{4}$$

where $g_j = (\partial \Phi^m / \partial y)_j$. The interface center point is denoted by index j and j + 1/2 signifies cell center (d). Application of the compact scheme to all cell interfaces in the domain produces an algebraic set of equations which can be solved by a standard tridiagonal solver. The required boundary conditions are determined from the respective velocity update equation (2b). For example, application of equation (3) at cell interface i = S in Figure 1 requires a boundary definition for f_{i-1}. This definition is supplied by the velocity update equation as

$$\frac{\left(u^{n,m}_{i-1} - \hat{u}^m_{i-1}\right)}{\Delta t} = -\left(\frac{\partial \Phi}{\partial x}\right)^m_{i-1} = -f_{i-1}, \tag{5}$$

where $u^{n,m}_{i-1}$ and $\hat{u}^m_{i-1}$ are the averaged velocity boundary values centered between grid points 1 and 4. The pressure gradient g_{j-1} in equation (4) is treated similarly. There

$$\frac{\left(v^{n,m}_{j-1} - \hat{v}^m_{j-1}\right)}{\Delta t} = -\left(\frac{\partial \Phi}{\partial y}\right)^m_{j-1} = -g_{j-1}, \tag{6}$$

where $v_{j-1}^{n,m}$ and $\hat{v}_{j-1}^{m}$ are the averaged velocity boundary values centered between grid points 1 and 2. Finally, one should note that the pressure gradients for updating the w-velocity components are computed in an analogous manner.

The intermediate velocity equation is solved by using the approximate-factorization technique. Because this equation is not coupled explicitly to the pressure-Poisson equation in terms of the scalar Φ^m, it is solved only once for each intermediate velocity component at the outset of each Runge-Kutta step. Thus, the computational efficiency of this fractional-step technique is governed primarily by the CPU time required to solve the pressure-Poisson equation. This equation satisfies the incompressible constraint to within a user-specified error tolerance, and its rapid convergence by an iterative scheme is essential to the overall solution procedure. For this purpose the modified strongly implicit (MSI) scheme, developed by Schneider and Zedan [15], is implemented in a residual form of the pressure-Poisson equation. The computational efficiency of the MSI scheme over point-successive relaxation and alternating directional implicit techniques was demonstrated by Jordan and Spaulding [16] for 2D grid-generation and by Jordan [17] for solving the vorticity-stream function equations in 2D steady-state flow problems. Extension of this solver to the 3D pressure-Poisson equation is a straightforward process. It can be viewed as an implicit solver of a planar surface (either x-y, x-z or y-z) that passes through the computational volume in a direction (z, y or x, respectively) which is normal to the surface. The 2D solver sweeps through the volume analogous to the manner an implicit line solver sweeps along a planar surface.

The residual form of the discretized pressure-Poisson equation appears as

$$[A_1 + A_2 + A_3]\delta^{\ell+1} = -R^{\ell}, \tag{7}$$

where the coefficient matrix has components $A_i = \delta^2 / \delta x_i^2$, the increment $\delta^{\ell+1} = \Phi^{m,\ell+1} - \Phi^{m,\ell}$ and R^{ℓ} is the residual. The parameter ℓ denotes successive updates to the variable Φ^m and m is the particular Runge-Kutta step.

For the pressure-Poisson equation, the residual is defined as

$$R^{\ell} = \frac{\partial^2 \Phi^{m,\ell}}{\partial x_i \partial x_i} - \frac{1}{\Delta t}\frac{\partial \hat{u}_i^m}{\partial x_i}. \tag{8}$$

Solution of the increment δ in equation (7) by the MSI scheme is a three-step process which constitutes a single iteration ℓ. Each step reflects a single sweep of the solution scheme through the computational volume. The directional order of each sweep is irrelevant to the final solution, although the number of total iterations required for convergence may sometimes be

affected. The three-step sequence chosen here is in the order of z,x,y and has the form

$$\left(A_i + A_j\right)\delta^{\ell+1} = -R^{\ell}, \tag{9}$$

where i,j are cyclic indices. For quickest convergence, the residual is recomputed after each sweep. The full 3D solution is now dimensionally reduced to three 2D implicit solutions for which the MSI scheme is directly applied. Convergence is monitored by computing the root-mean-square (RMS) of the residual. At convergence $R^{\ell}_{RMS} \cong 0$ meaning that the incompressibility constraint has been satisfied to within the error tolerance specified by the user.

By factoring the coefficient matrix in this way, the MSI scheme can be implemented easily. This scheme was originally designed by Schneider and Zedan [15] as a nine-point implicit solver which makes it well-suited to handle a 2D curvilinear form of the pressure-Poisson equation. But by conveniently eliminating the appropriate components, it can be applied effectively to the 2D Cartesian coordinate system. If the pressure-Poisson equation is recast into a residual form first, rather than implementing the MSI scheme directly, the solution methodology gains several distinct advantages. From an accuracy standpoint, the residual which is a necessary computation in the residual form is a justified gauge for monitoring convergence. Also, from a programmer's viewpoint, implementation of the MSI scheme is greatly simplified. This is because the residual term is zero-valued everywhere on the grid boundaries; therefore tracking those boundaries in the computation is not necessary. This latter advantage is particularly important when computing flow in domains having internal boundaries.

BOUNDARY CONDITIONS

The impetus for collocating the velocity components with the grid points is to facilitate derivation of a consistent set of boundary conditions for the intermediate velocity components along no-slip walls. For the semi-staggered grid, a proper definition for the intermediate velocity along no-slip wall boundaries begins by projecting equation (2a) onto the wall. The result is

$$\hat{u}_i^m - u_i^{n,m-1} = \frac{\gamma^m \Delta t}{Re} \frac{\partial^2\left(\hat{u}_i^m + u_i^{n,m-1}\right)}{\partial x_j \partial x_j}, \tag{10}$$

which is implicit in $\hat{u}_i^m$. The components of $\hat{u}_i^m$ can be approximated in terms of $\hat{u}_i^{m-1}$ up to second-order accuracy in time by noting that

$$u_i^{n,m} - \hat{u}_i^m = -\Delta t \nabla \Phi^{m-1} - O(\Delta t)^2 = u_i^{n,m-1} - \hat{u}_i^{m-1} - O(\Delta t)^2. \qquad (11)$$

Since $u_i^{n,m} = u^{n,m-1}$ along the wall, equation (11) shows that $\hat{u}_i^m = \hat{u}_i^{m-1} + O(\Delta t)^2$. By substituting this result into equation (10), the definition for the intermediate velocity becomes

$$\hat{u}_i^m - u_i^{n,m-1} = \frac{\gamma^m \Delta t}{Re} \frac{\partial^2 \left(\hat{u}_i^{m-1} + u_i^{n,m-1} \right)}{\partial x_j \partial x_j} + O(\Delta t)^3, \qquad (12)$$

which is consistent with the temporal accuracy of the field solution. To maintain the same spatial accuracy along the boundary as in the field, the diffusive term is approximated by second-order-accurate one-sided differences. The consistency and accuracy of this boundary condition is tested in the next section.

Two important concerns are satisfied by staggering the pressure variable in the computational molecule. Besides inhibiting spurious oscillations in the numerical solutions [13], no ad hoc wall boundary conditions are necessary for the pressure variable. This can be illustrated effectively by the following simple example. The residual for the one-dimensional form of the discretized pressure-Poisson equation at the center cell point i = a in Figure 1 is

$$R^{\ell} = \left(\Phi_{i-1} - 2\Phi_i + \Phi_{i-1} \right)^{\ell,m} - \frac{\Delta x}{2\Delta t} \left[\left(\hat{u}_5 + \hat{u}_2 \right) - \left(\hat{u}_4 + \hat{u}_1 \right) \right]^m. \qquad (13)$$

The u-velocity update equation applied at the no-slip wall $\left(u_i^n = 0 \right)$ to the left of grid cell (a) becomes

$$\frac{\Delta x}{2\Delta t} \left(\hat{u}_4 + \hat{u}_1 \right)^m = \left(\Phi_i + \Phi_{i-1} \right)^{\ell,m}. \qquad (14)$$

Substitution of this equation into equation (13) in terms of $\left(\hat{u}_4 + \hat{u}_1 \right)$ reveals that the evaluation of the residual closest to the wall boundary does not require an ad hoc definition for the pressure variable at the wall (or outside the wall) in terms of the field values. As a consequence, the pressure field remains conservative and second-order accurate, and the rate of convergence significantly improves because an ad hoc definition commonly appears as a Neuman type boundary condition. Extension of this example to three-dimensions will yield the same result.

SOLUTION ACCURACY

The temporal and spatial accuracy of the overall solution procedure as well as the consistency of the intermediate velocity boundary conditions can

be verified by simulating an exact solution of the 2D unsteady NS equations. Through reduction of the mesh spacing under a constant CFL value, the numerical results should display second-order improvement as given by the leading truncation error. The exact solution has the form [1]

$$u(x,y,t) = -\cos(x)\sin(y)e^{-2t} \tag{15a}$$

$$v(x,y,t) = \sin(x)\cos(y)e^{-2t} \tag{15b}$$

$$p(x,y,t) = -\tfrac{1}{4}[\cos(2x)+\cos(2y)]e^{-4t} \tag{15c}$$

The simulation was initialized by the exact solution for time t = 0.0. The spatial domain was defined as $0 \le x,y \le \pi$. Using an exact set of boundary conditions for the physical velocity with the definition in equation (12) for the intermediate velocity (including convection where appropriate), the initial flow field was advanced to the same physical time for each grid tested. In this case, t = 0.35 seconds, which corresponds to a reduction of the maximum boundary velocity to one-half of its initial value. The results are plotted in Figure 2 where the grid factor is the ratio of the grid spacing in the reference grid (11 x 11 uniform) to the refined grid. An exact error was determined as the absolute maximum difference between the numerical predictions and the exact solution normalized by the maximum value in the domain. Figure 2 clearly shows a linear reduction of the velocity and pressure errors by refining the grid. These reductions indeed signify a technique which is second-order accurate. Thus, the numerical accuracy of the solution technique is verified along with the consistency of the boundary conditions for the intermediate velocity.

NUMERICAL STABILITY

Many previous applications of the fractional-step method to unsteady viscous flows temporally discretized the convective term by the Adams-Bashforth method (see Antonopoulos-Domis [18] and Kim and Moin [9] for example). This scheme holds the advantages of being second-order-accurate, one-step and low-storage (only information from the previous time step needs to be saved). Unfortunately, a Fourier stability analysis will reveal that the method is unconditionally unstable if applied to the linear convection equation. As shown in Figure 3 however, this instability is weak for Courant numbers less than 0.5 which explains why the method has been successful for solving viscous flow problems. But for certain viscous flow problems where at some point $Re \to \infty$ during the simulation, for example in an impulsively started flow, very small CFL values would be necessary (at the outset in this example) to sustain stable solutions.

The fractional-step technique developed here is expected to posses strong stability characteristics. As pointed out earlier, a third-order-accurate three-step low-storage Runge-Kutta procedure was chosen to meet

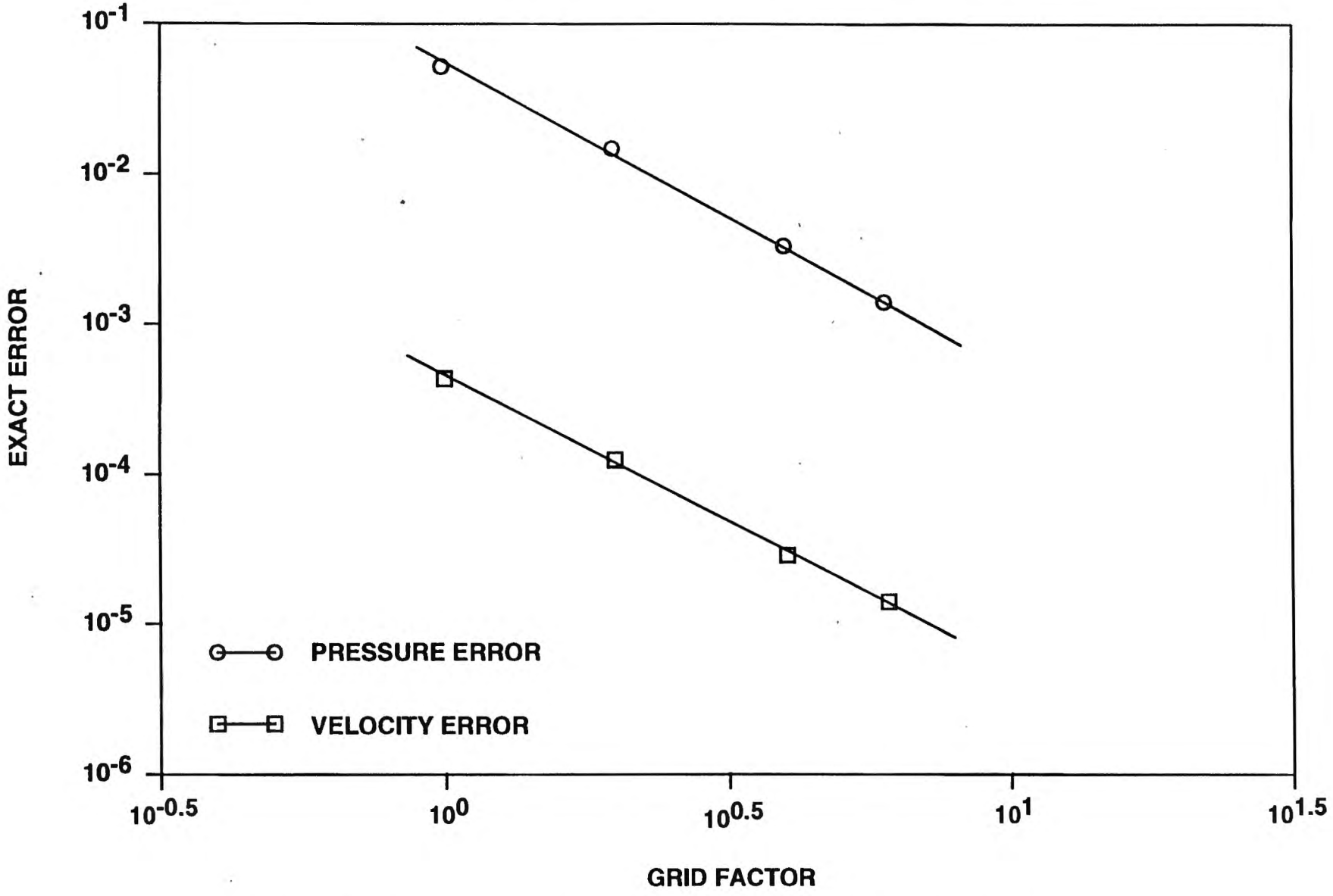

Figure 2. Improvement in the Exact Errors of Velocity and Pressure with Grid Refinement for a Constant Courant Number

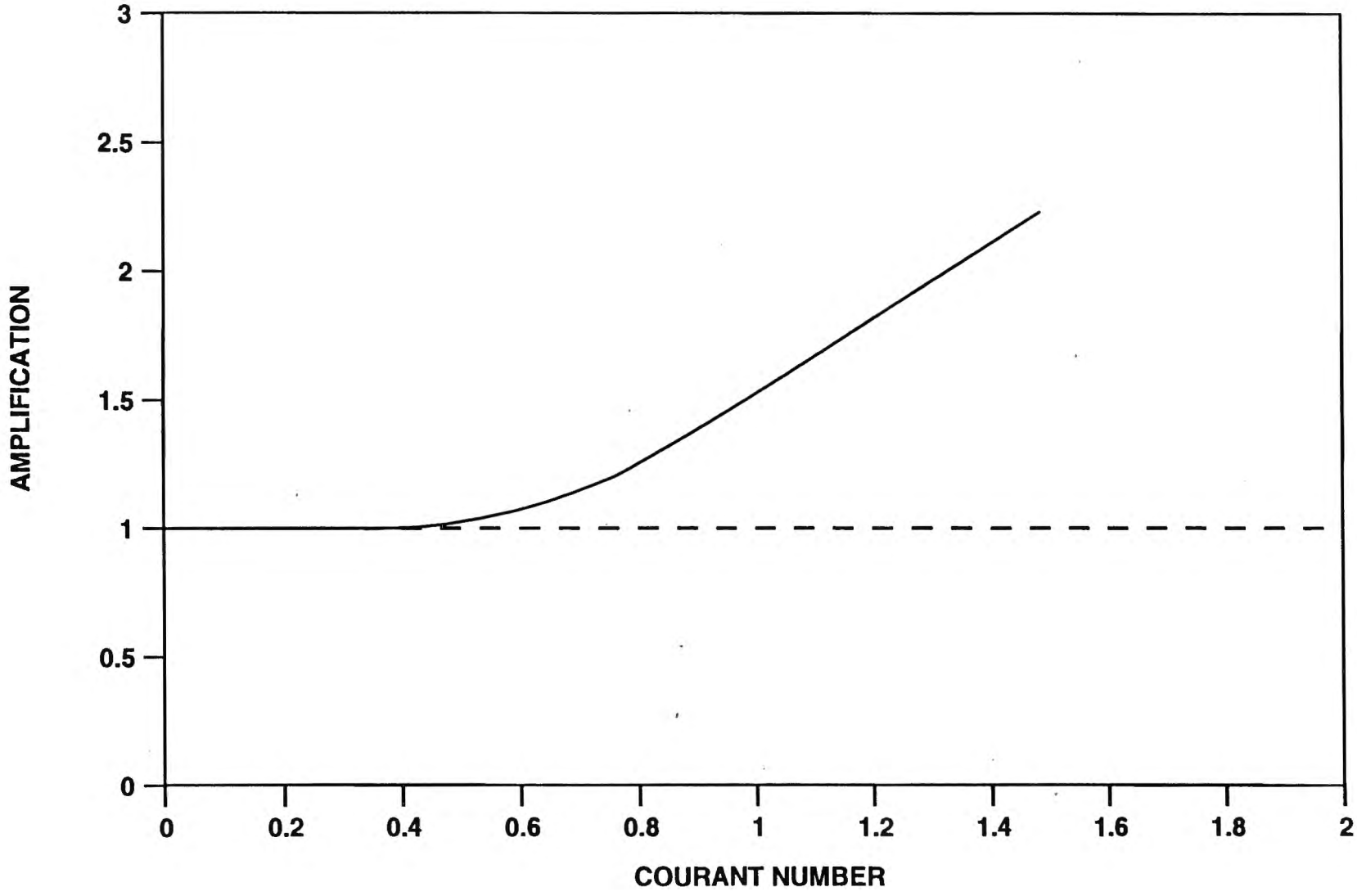

Figure 3. Numerical Stability of the Adams-Bashforth Method Applied to the Linear Convection Equation

this need in lieu of the Adams-Bashforth method. This procedure is conditionally stable when applied to the linear convection equation. As shown in Figure 4, when the procedure is combined with third-order-accurate upwind-biased spatial differences, the linear convection equation is always stable for Courant numbers $\sigma \leq 1.6$. In the case of the impulsively started flow problem, reasonable time increments would be permitted early in the simulation. Obviously, as the relative importance of a viscous term increases, the stability limit shown in Figure 4 would be relaxed.

RESULTS AND DISCUSSION

In this section we present the simulation results of a 3D shear-driven cavity flow at moderate Reynolds numbers of 2000 and 3200. At these Reynolds numbers the flow is unsteady and fully laminar. In the discussion of the numerical results, we include qualitative and quantitative comparisons to the experimental data previously published. Rhee et al [19] published flow visualization results of the cavity flow at Re = 2000 and Re = 3300 while Koseff and Street [20,21] presented extensive visualization and statistical flow data at Re = 3200. In those experiments, the cavity width (x-direction) equaled the height (y-direction). The length of the span (z-direction) was varied. The visualization evidence showed that the 2D recirculation flow (x-y planes) can be characterized basically by a primary vortex, a downstream secondary eddy, an upstream secondary eddy and an upper secondary eddy (see Figure 5). These basic features have been predicted many times by solution techniques that solved the classic 2D problem (see Ghia et al [22] for example). In the spanwise direction, the flow forms Taylor-Gortler-like (TGL) vortex pairs and a lower corner vortex at the spanwise end-walls. These characteristics are illustrated in Figure 6. According to Koseff and Street [23], the impetus manifesting the TGL vortices is the instability of the concave free shear layer that separates the primary vortex from the downstream secondary eddy. These vortices form just above the concave surface much like the flow experiments between rotating cylinders by Taylor [24] and the concave boundary layer investigation by Gortler [25]. At the Reynolds numbers under consideration, the visualization results showed the TGL vortices meandering slowly along the cavity bottom. The size and number of vortices depends strongly on the Reynolds number. However, Rhee et al [19] and Koseff and Street [20,22] noted that the spanwise flow was symmetric about the mid-span plane when the spanwise aspect ratio (SAR) of the experimental apparatus was extended to three. Manifestation of the corner vortex is a consequence of the shear and pressure force adjustment in the recirculating flow caused by the no-slip condition along the spanwise end-wall. Although this vortex is quasi-steady at these Reynolds numbers, its size and extent strongly influence the TGL vortices. Thus, sufficient grid resolution must be provided for both the TGL vortices and the corner vortex to properly capture the characteristics of this truly unsteady flow.

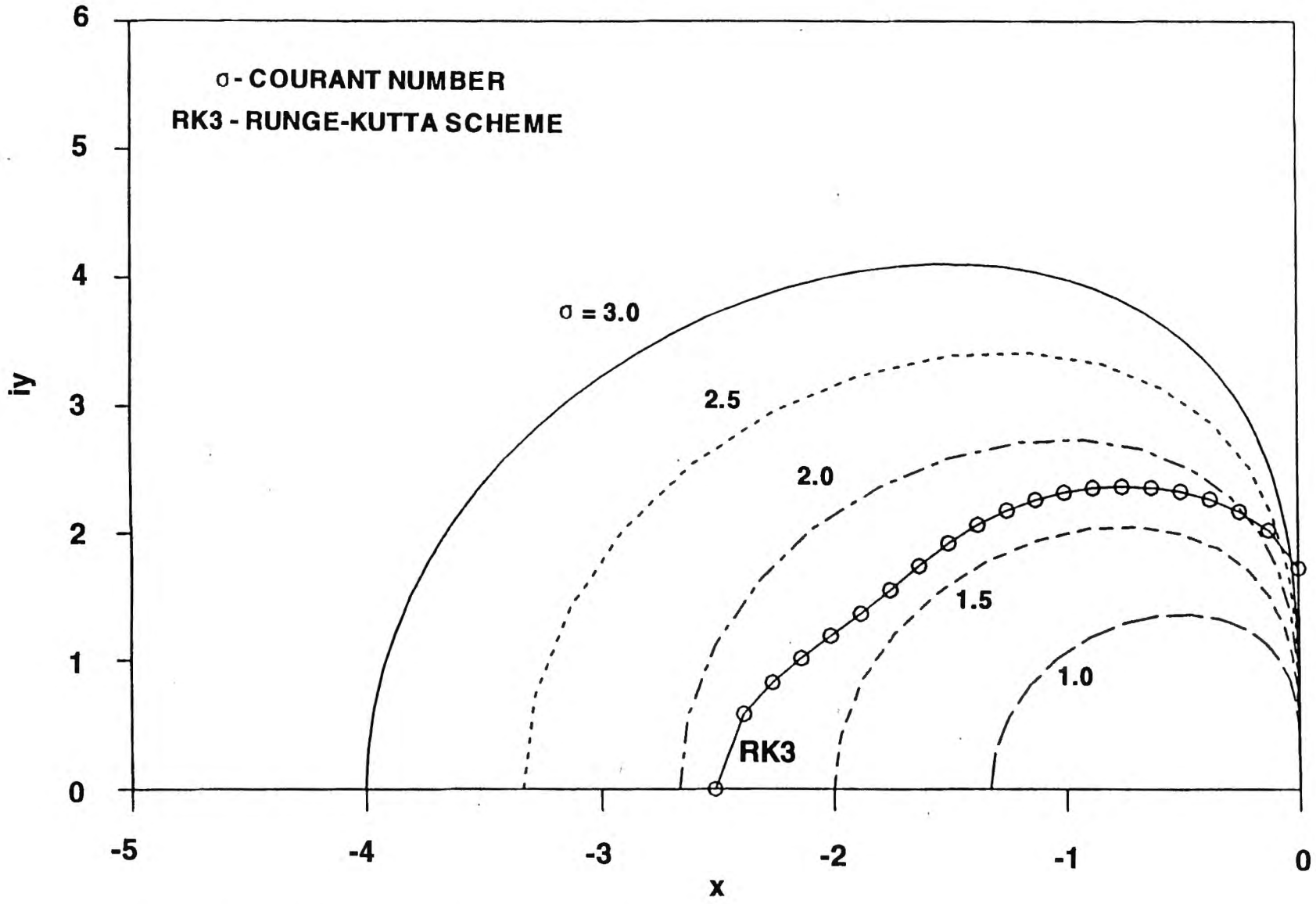

Figure 4. Numerical Stability of the Linear Convection Equation Using the Third-Order-Accurate Three-Step Runge-Kutta Procedure and Third-Order-Accurate Upwind-Biased Spatial Differences

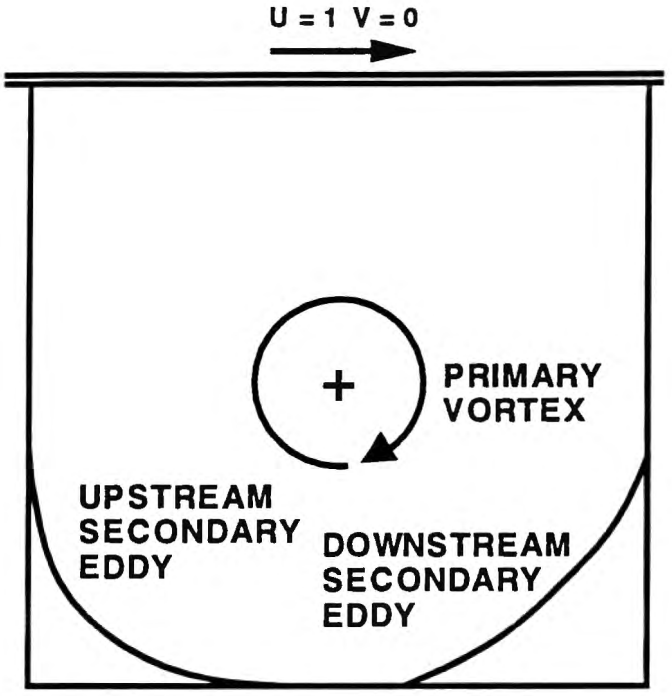

Figure 5. Sketch of the Basic Features of Recirculation in the Two-Dimensional Shear-Driven Cavity Flow Problem

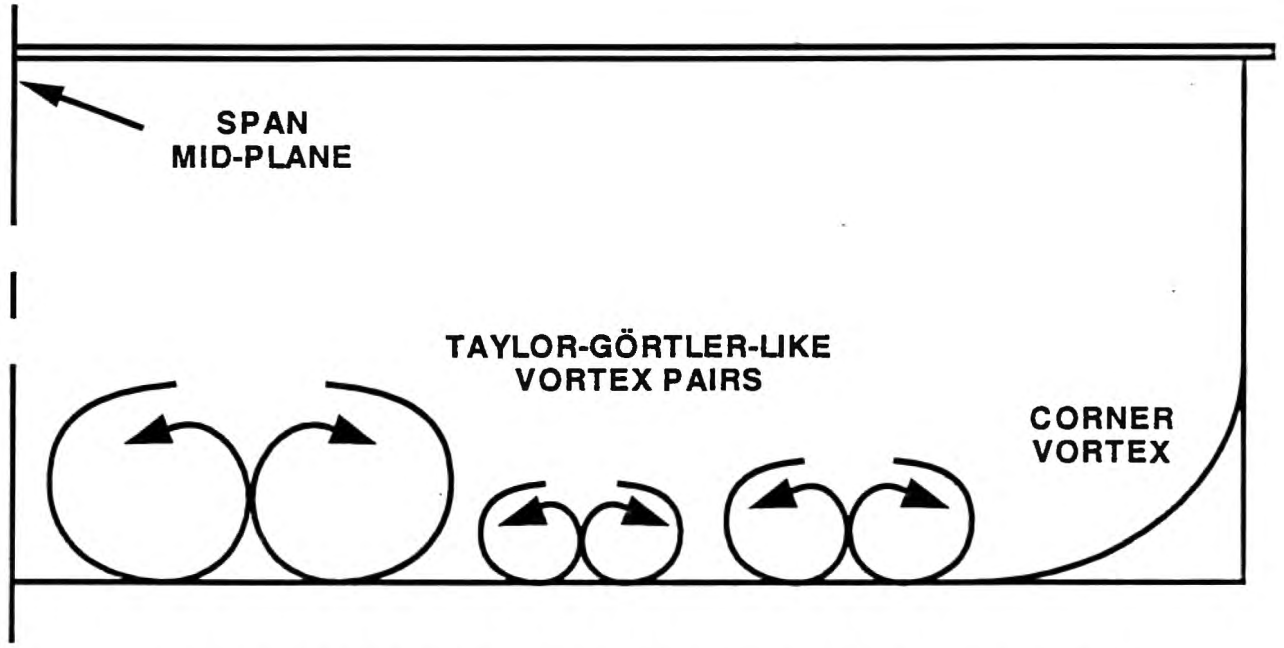

Figure 6. Sketch of the Taylor-Gortler-Like Vortex Pairs as Observed in the Flow Visualization Experiments

In both simulations of the 3D shear-driven cavity flow , the geometry was modeled with unit width and unit height (see Figure 7). The span length was 1 and 1/2 times that of the width (or height) with one boundary modeled as a plane of symmetry at the mid-span and the other a solid end-wall; thus as in the experiments, SAR = 3.0. The cavity lid moved horizontally at unit velocity and the no-slip condition was applied to all boundaries except the mid-span plane which was treated numerically as a plane of symmetry. Each simulation was initialized by an impulsively started lid. Extremely small time steps were not necessary early in the computation which was due to the use of the Runge-Kutta procedure. The results labeled t = 0.0 depict solutions that had been time-advanced until the transient effects of the impulsively started lid became negligible. After completion of the early time steps, only a few iterations of the pressure-Poisson equation were necessary to reach incompressibility at each new time level.

For the cavity flow test case at Re = 2000, a 41 x 41 x 51 uniform grid (x, y, z directions) was used with CFL = 2.4. A high resolution in the spanwise direction was chosen to insure prediction of the complete TGL vortex structure. Three sets of snapshots are shown in Figure 8 of the recirculation and spanwise flow at non-dimensional times of t = 0.0, 8.0 and 16.0. The recirculation velocity vectors typify the flow at the mid-span plane. For clarity, they are normalized with respect to their own magnitudes. The spanwise velocity vectors show the flow at a plane where x $\cong$ 0.77. The relative time t = 0.0 is an actual time of 24 seconds after impulsive start of the cavity lid. At this initial time, three small TGL vortex pairs span the cavity bottom with a large corner vortex located at the lower end-wall. The corresponding recirculation flow displays strong 2D features which is a consequence of the weak spanwise flow. After an additional eight time units however, the TGL vortex closest to the mid-plane nearly doubled its physical size. This now larger vortex pair impacts the recirculation flow locally by extracting kinetic energy from the downstream region; consequently reducing the size of the downstream secondary eddy. At time t = 16.0, three TGL vortices clearly appear with a fourth much weaker one positioned near the corner vortex. The prediction of four TGL vortices at Re = 2000 agrees with the flow visualization results reported by Rhee el al [19].

In the flow visualization experiments at this Reynolds number, the TGL vortices meandered slowly along the cavity bottom as well as varied their physical size. This behavior is also illustrated in Figure 9 where five snapshots of the computations are shown at unit time intervals beginning with t = 26. The sequence of snapshots show creation and stationary growth of a TGL vortex pair directly next to the mid-span plane. Conversely, the TGL vortex closest to the end-wall is reduced and reverses its lateral path three times. Furthermore, this particular vortex meanders across approximately 15 percent of the cavity bottom. The remaining two TGL vortices also display large variations in their physical size, but meander comparatively to a much lesser degree.

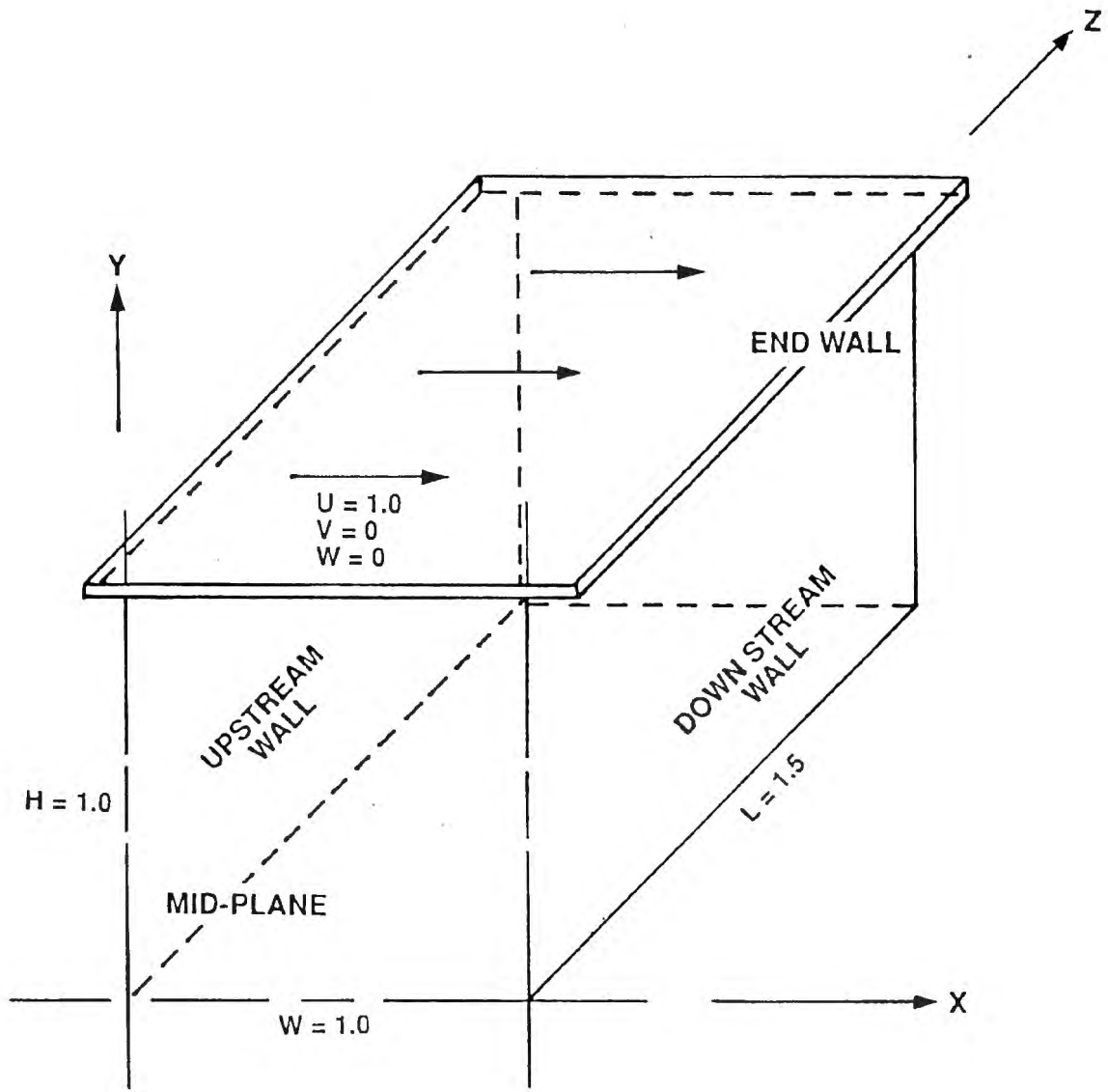

Figure 7. Model Problem for Present Predictions of the Shear-Driven Cavity Flow

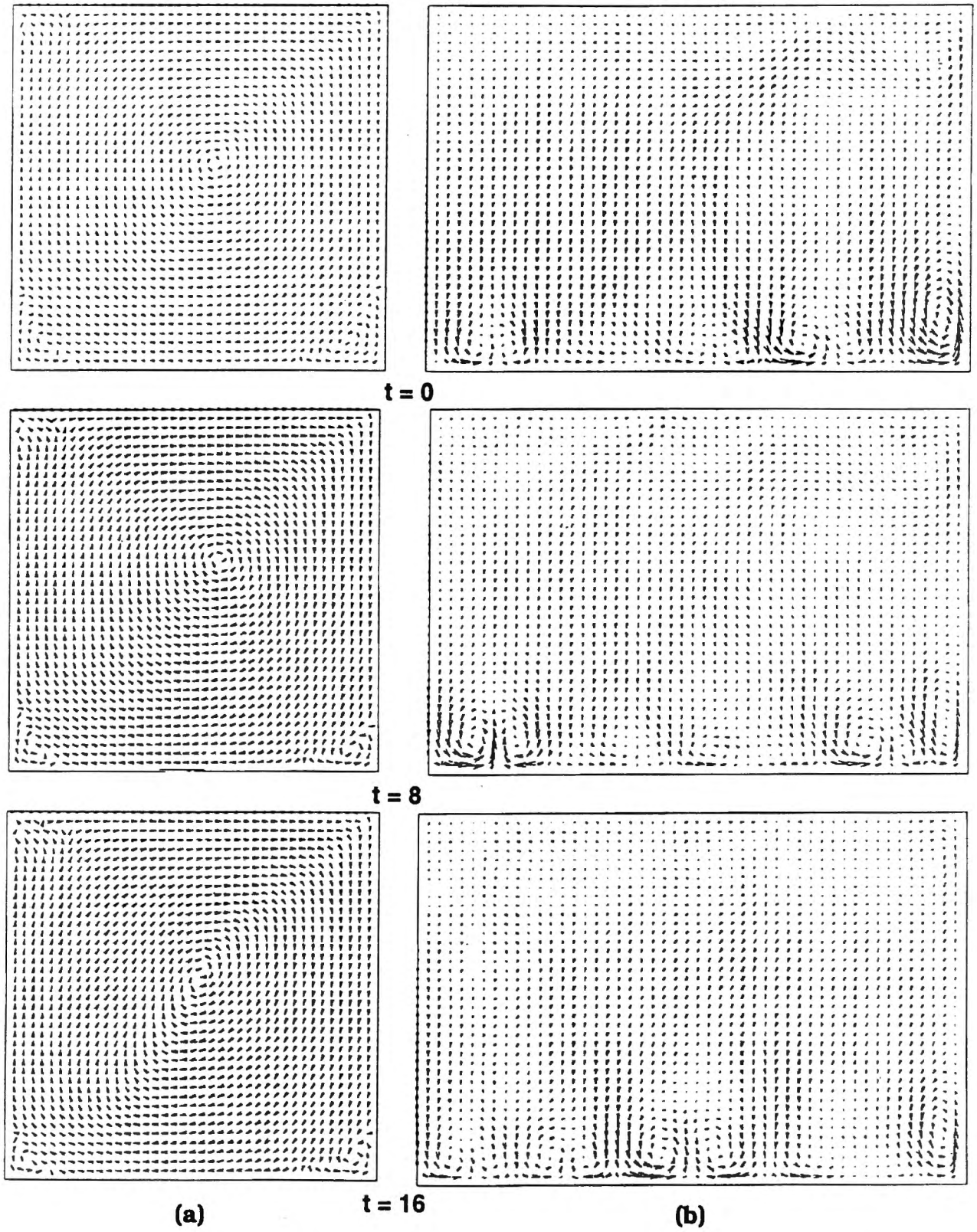

Figure 8. Snapshots of the Recirculation (a) and Spanwise Flow (b) in the Three-Dimensional Shear-Driven Cavity at Times t=0.0, 8.0 and 16.0 for Re = 2000 and a 41 x 41 x 51 Uniform Grid. Recirculation Vectors are Shown at the Cavity Mid-Span Whereas Spanwise Flow is at Plane X = 0.77

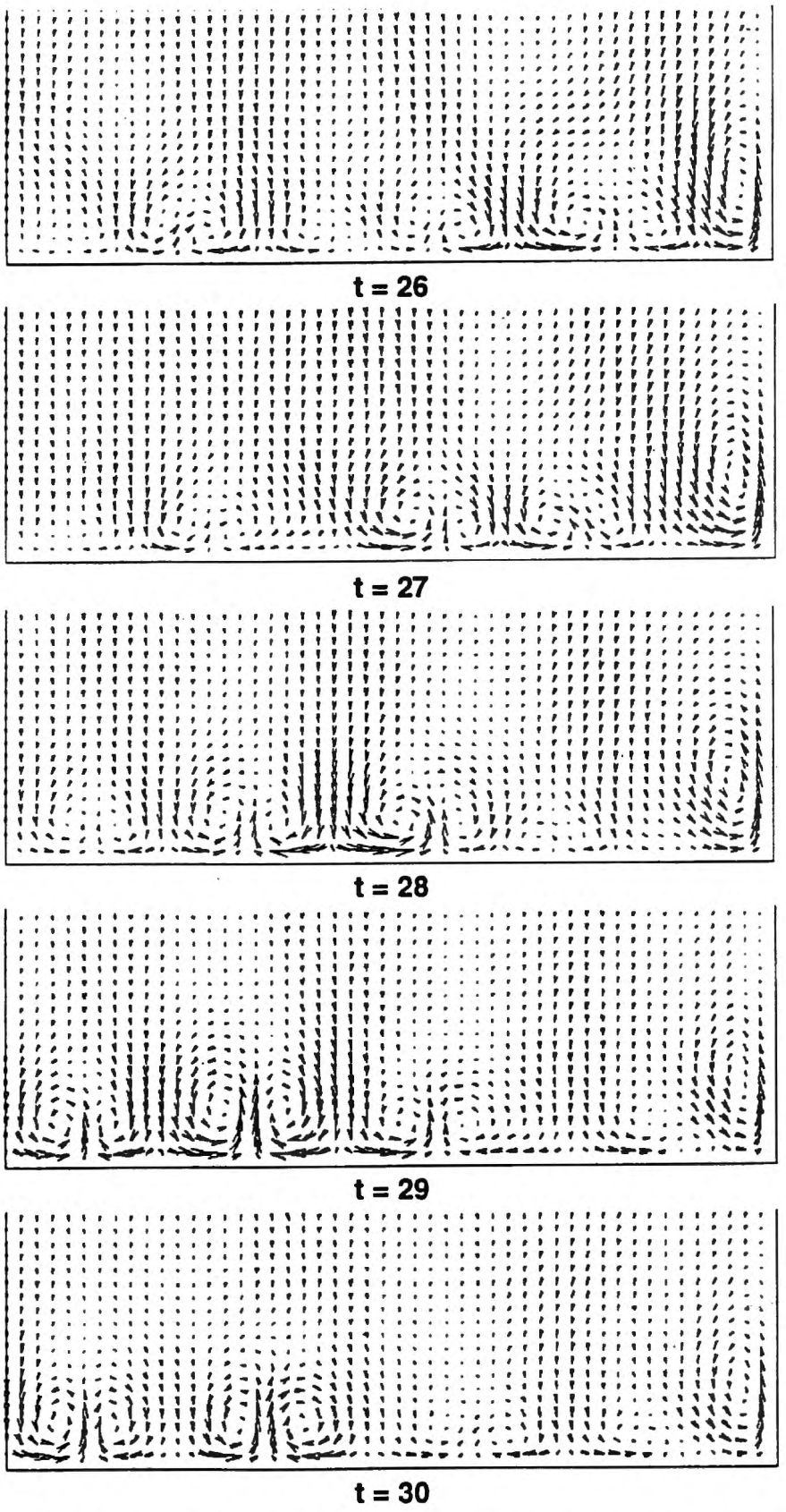

Figure 9. Snapshots of Spanwise Flow Showing Meander and Physical Size of TGL Vortices for Re = 2000 Test Case

To graphically verify the claim of strong coupling between the velocity components and pressure variable, three pressure variable profiles are displayed in Figure 10. The pressure variable is plotted instead of the actual pressure to avoid the natural smoothing of the diffusive term as given in equation (2d). The profiles represent cuts at $y = 0.1$ through the free shear layers that separate the primary vortex from the secondary eddies. These profiles extend from the upstream wall ($x = 0.0$) to the downstream wall ($x = 1.0$) at the mid-, 1/3rd and 2/3rds planes along the cavity span. Notice that the profiles depict smooth continuous curves that are devoid of spurious oscillations. These characteristics illustrate proper coupling between the pressure variable and velocity components as given by the discretization molecule.

A 51 x 51 x 65 uniform grid was selected for the test case at Re = 3200 and a CFL value of 1.5. This mesh resolution was based on the simulation reported by Freitas et al [12] where a 32 x 32 x 45 grid was used that was non-uniform in the recirculation planes. A lower CFL value was chosen for this test case to insure capture of the unsteady flow physics in the cavity. Figures 11a and 11b show typical snapshots of the unsteady flow ($t = 12.0$). The recirculation velocity vectors (Figure 11a) represent the flow at the mid-span plane whereas the spanwise flow (Figure 11b) is shown at the $x \cong 0.77$ plane. Once again for clarity, the recirculation velocity vectors are normalized with respect to their own magnitudes. Four TGL vortex pairs span the cavity bottom. Their position is marked by grid lines referenced to the cavity mid-span. This number of TGL vortices agrees with the experimental observations reported by Rhee et al [19]. The streamwise extent of each vortex pair in the form of x-vorticity contours is plotted in Figure 12. The marking of grid lines in that figure and in the spanwise velocity vectors (Figure 11b) help quantify the intensity of each vortex with respect to its spanwise size and streamwise extent. Generally, the streamwise stretch of each vortex is directly dependent on its size and strength. As time passes however, new TGL vortices are generated which gain physical strength and size. Also, the corner vortex over the same time period behaves in a similar manner. For example, the snapshots in Figure 13 ($t=75.0$) shows a large TGL vortex straddling the mid-span with three smaller ones along the spanwise plane. The larger TGL vortex clearly dominates the local downstream region of the cavity near the mid-span by completely eliminating development of the secondary eddy. Normalized recirculation velocity vectors representing 18 minute sample averages at the 1/3rd and 2/3rds planes from the spanwise end-wall are shown in Figures 13a and 13b, respectively. At these planes, downstream and upstream secondary eddies are clearly visible, but not an upper secondary eddy. Freitas et al [12] also reported this result and both results agree with the flow visualization data [19,20]. Furthermore, the 1/3rd plane vectors show the primary vortex core positioned in the upper right quadrant of the recirculation plane whereas the core at the 2/3rds plane lies close to the geometric center. This result also agrees qualitatively with the experimental observations and is due to the proximity influence of the end-wall on the recirculation flow.

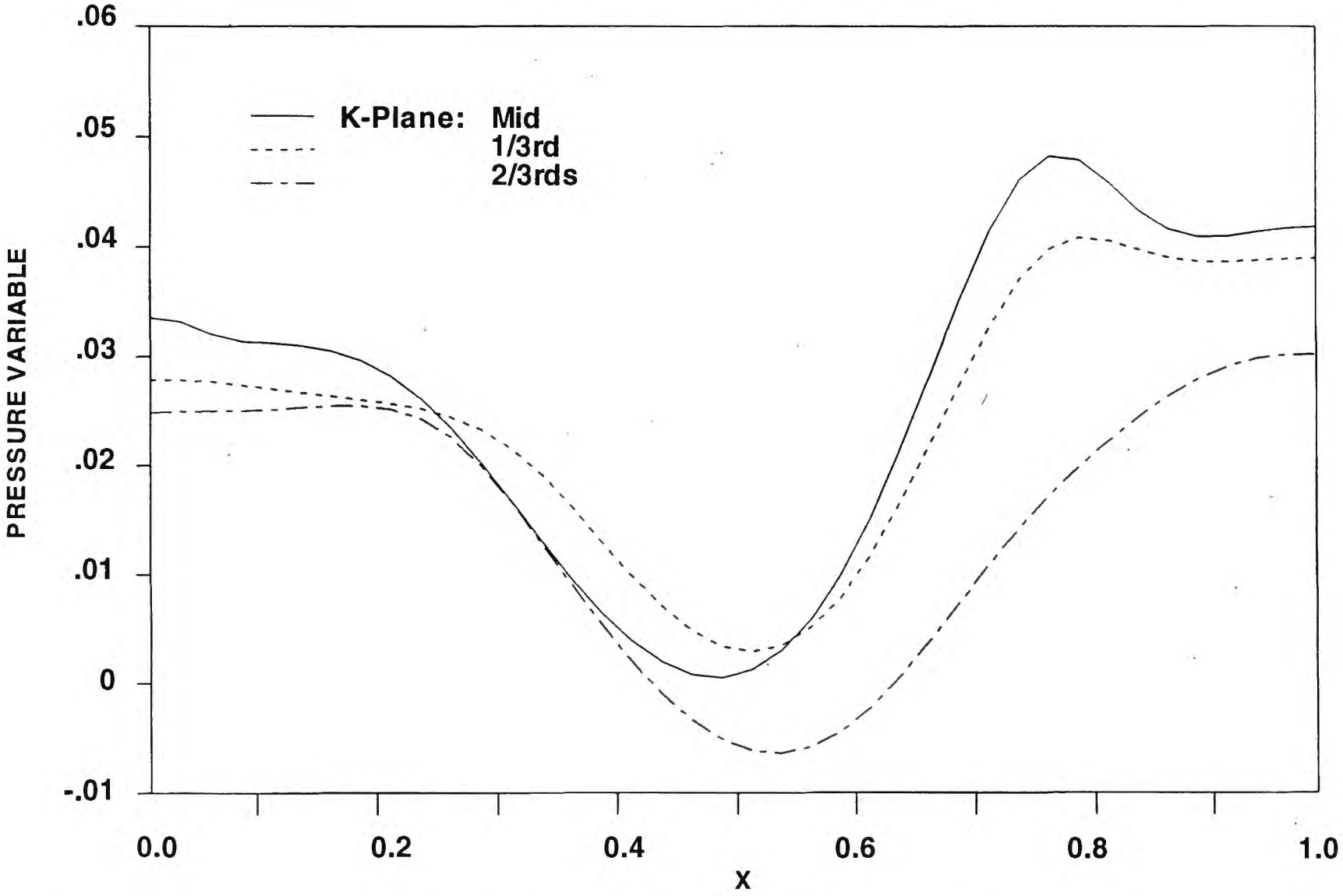

Figure 10. Pressure Variable Profiles at Y = 0.1 from the Upstream (x = 0.0) to the Downstream Wall (x = 1.0) at the Mid, 1/3rd and 2/3rds Planes in the Z Direction

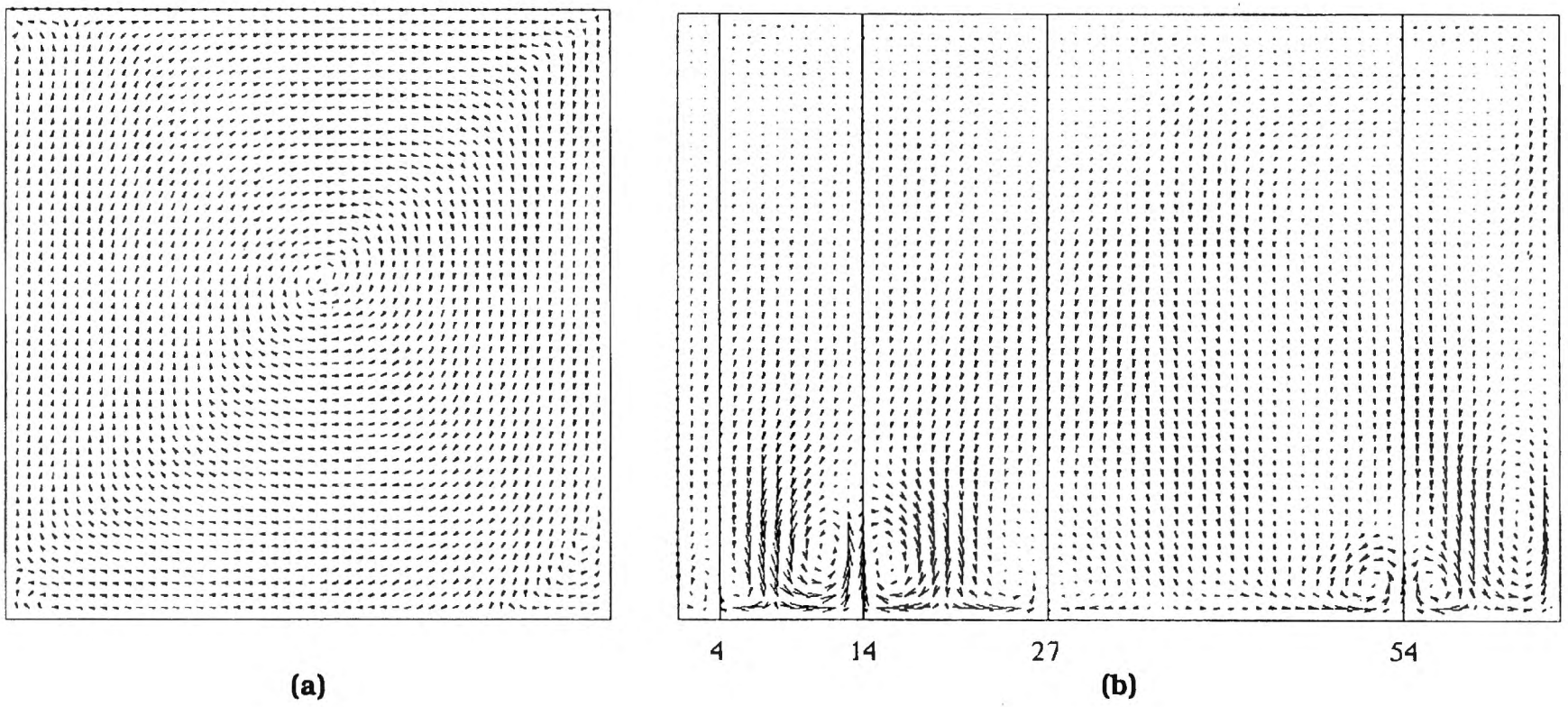

Figure 11. Snapshots of the Recirculation (a) and Spanwise Flow (b) in the Three-Dimensional Shear-Driven Cavity at Time t=12.0 for Re = 3200 and a 51 x 51 x 65 Uniform Grid. Recirculation Vectors are Shown at the Cavity Mid-Span Whereas the Spanwise Flow is at Plane X = 0.77

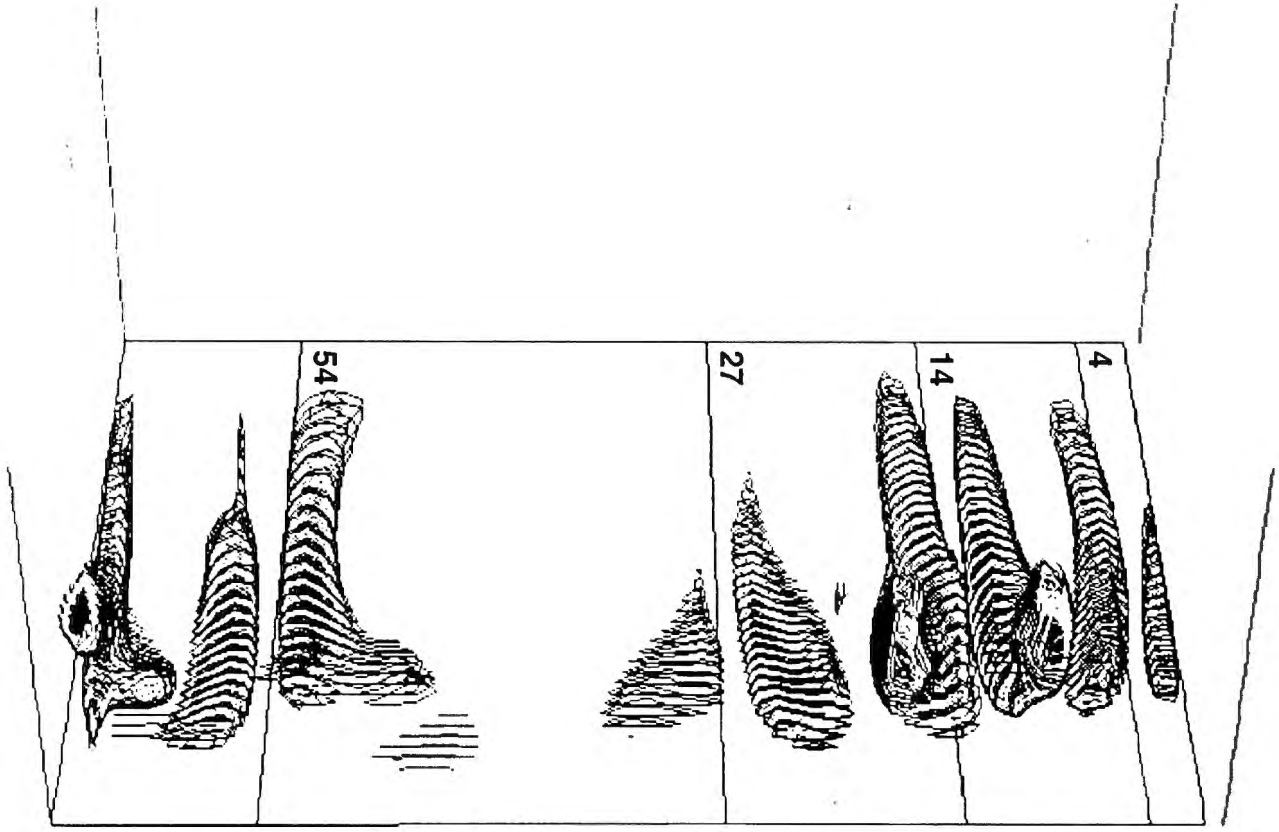

Figure 12. X-Vorticity Contours of Spanwise Flow in Shear-Driven Cavity at Re=3200. Grid Line Numbers Coincide with Numbers in Figure 11b

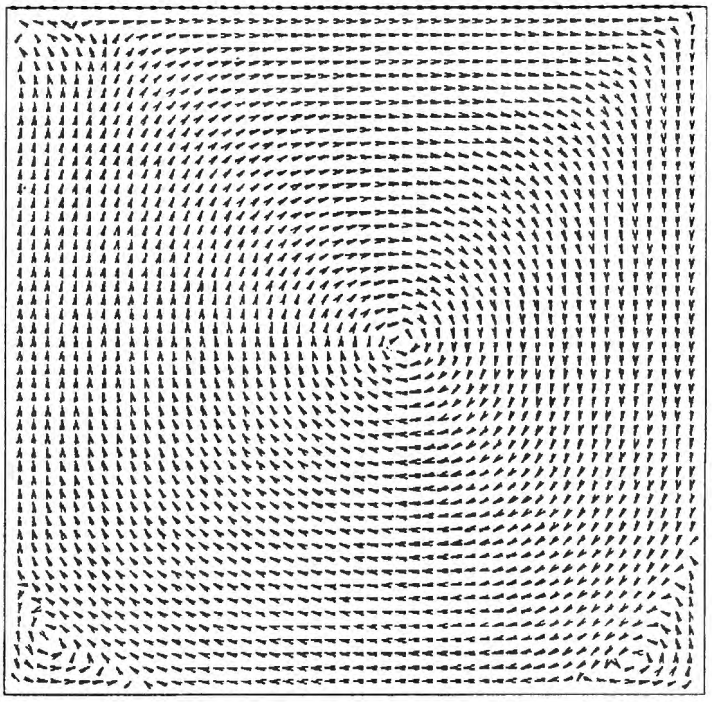

(a)

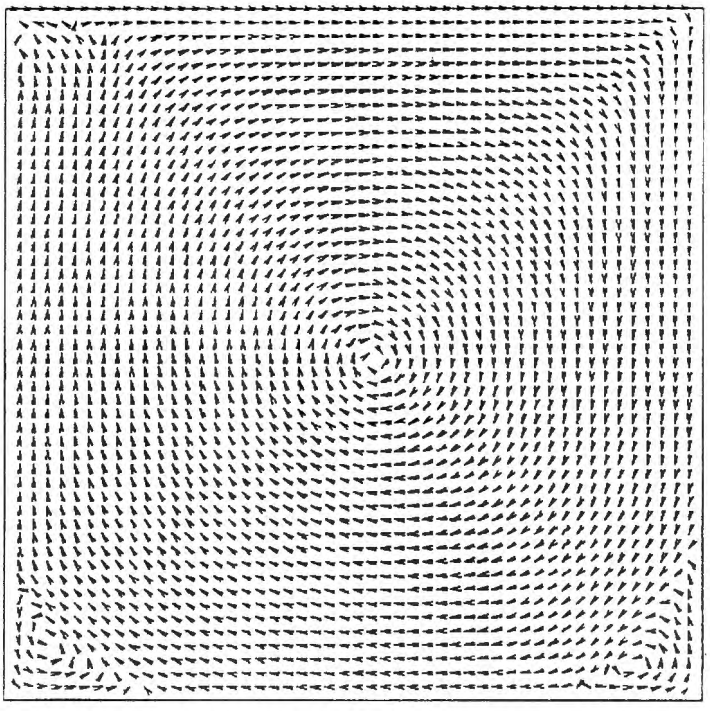

(b)

Figure 13. Normalized Recirculation Velocity Vectors Representing 18-Minute Sample Averages of Shear-Driven Cavity Flow at Re = 3200; (a) 1/3rd and (b) 2/3rds Planes from the Cavity Spanwise End-Wall

The experimental and computed time-averaged u and v velocity profiles through the cavity center at the mid-span are compared in Figures 14(a) and 14(b), respectively. The experimental profiles [20] represent five minutes of time-averaged measurements, whereas the present computations are averaged over 18 minutes. Also included in the figure are the steady 2D velocity profiles for a 51 x 51 uniform grid and the three minute time-averaged results of Freitas et al [12]. Comparisons between the 3D computations and experimental results are quite good. On the other hand, comparisons between the 2D computation and both 3D results are quite poor. This confirms the conclusion drawn by Koseff and Street [20], that the three-dimensional effects on the recirculation flow manifest significant differences between the 2D and 3D mean velocity profiles. One should note that the present time-averaged velocities away from the cavity walls agree better with the experimental data than the corresponding results of Freitas et al [12] for two possible reasons. The first is their lower sampling window, but more importantly, they sacrificed the grid field resolution by clustering lines near the cavity walls in the recirculation planes.

As a final note, after completion of the transient phase of the computation for this test case, the CPU requirement was approximately 1.3×10^{-5}s per grid point per Runge-Kutta step on a CRAY-YMP platform. This requirement compares competitively to the computational requirements reported by Kim and Benson [26]; 1.7×10^{-5}s (iterative time marching), 2.5×10^{-5}s (simplified marker-and-cell), and 4.5×10^{-5}s (PISO).

CONCLUSIONS

Details of a new fractional-step technique developed specifically for predicting three-dimensional unsteady incompressible flows was presented. Use of a semi-staggered grid pattern permitted easy derivation of a consistent set of boundary conditions for the intermediate velocity components without necessitating interpolation or extrapolation of the field data. Also, elimination of an ad hoc boundary condition for the pressure solution was demonstrated. The difficulty of insuring proper local coupling between the pressure and velocity components in the computational molecule was satisfied by computing the pressure gradient in the velocity update equation at the grid cell interfaces using fourth-order-accurate compact differences. Extension of the modified strongly implicit scheme for solution of the three-dimensional pressure-Poisson equation in residual form provided an efficient iterative means of quickly achieving incompressibility at each sub-step of the Runge-Kutta procedure. Both the consistency of the boundary conditions and global solution accuracy (second-order in time and space) were verified. The technique gave accurate qualitative and quantitative results of the three-dimensional shear-driven cavity flow at moderate Reynolds numbers of 2000 and 3200. The technique is also computationally competitive against other schemes of the same class.

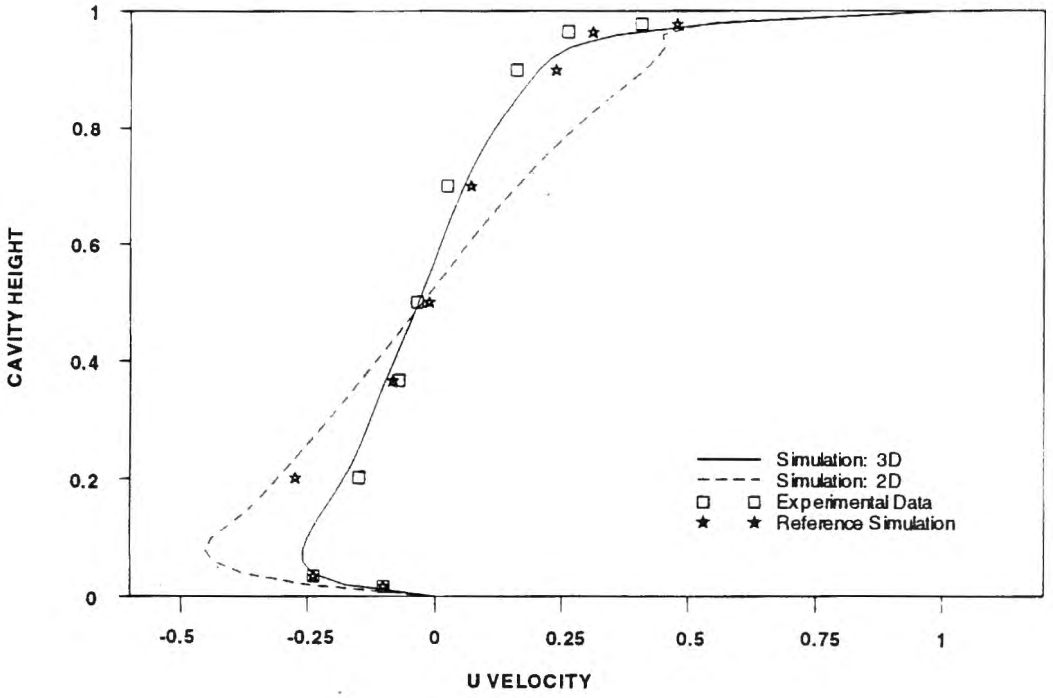

(a)

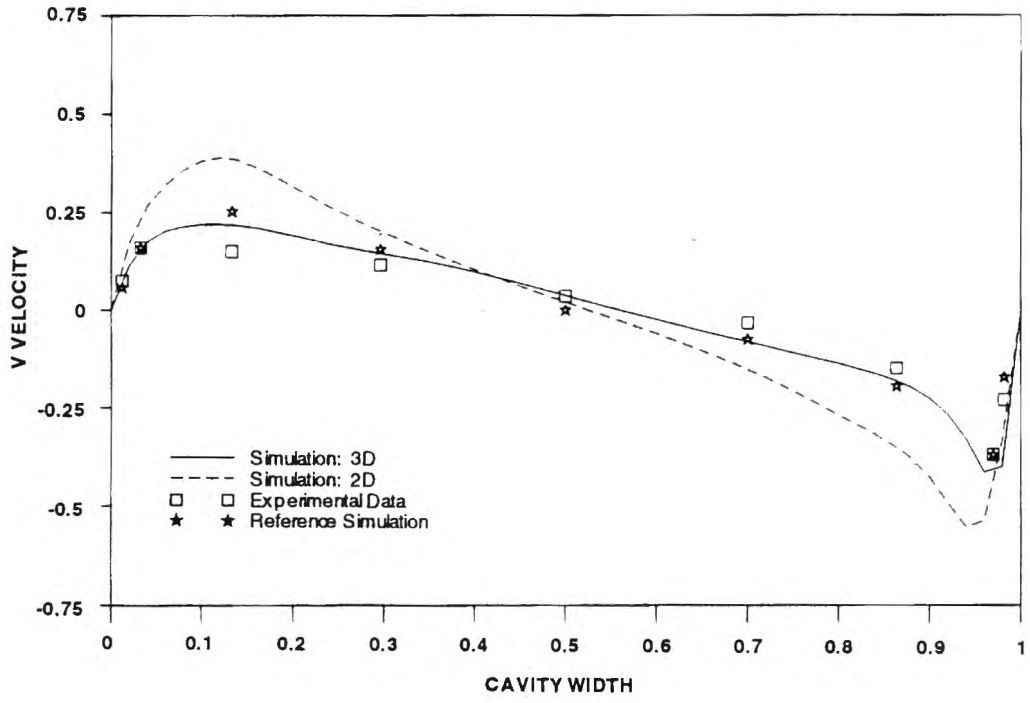

(b)

Figure 14. Comparison Between Experimental and Computational Time-Averaged Velocity Profiles Through Cavity Center at Mid-Span for Re=3200. Experimental Data Taken from Koseff and Street [21] and Reference Simulation from Freitas et al [12]: (a) u - velocity, (b) v - velocity

REFERENCES

1. A.J. Chorin, "Numerical Solutions of the Navier-Stokes Equations," Math. Comput., Vol. 23, 1969, pp 745-762.

2. R.I. Issa, "Solution of the Implicitly Discretised fluid Flow Equations by Operator-Splitting," J. Comp. Phys., Vol. 62, 1985, pp 40-65.

3. S.V. Patanka and D.B. Spalding, " A Calculation Procedure for Heat, Mass and Momentum Transfer in Three Dimensional Parabolic Flows", Int. J. Heat Mass Transfer, Vol. 15, 1972, pp. 1787-1806.

4. A. Wanik and U. Schnell, "Some Remarks on the PISO and SIMPLE Algorithms for Steady Turbulent Flow Problems," Comp. Fluids, Vol. 17, No. 4, 1989, pp. 555-570.

5. J.L.C. Chang and D. Kwak,"On the Method of Pseudo Compressibility for Numerically Solving Incompressible Flows," AIAA-84-0252, 1984.

6. A.J. Chorin, "A Numerical Method for Solving Incompressible Viscous Flow Problems", J. Comp. Phys., Vol. 2, 1967, pp 12-26.

7. W.Y. Soh and J.W. Goodrich, "Unsteady solution of Incompressible Navier-Stokes Equations", J. Comp. Phys., Vol. 79, 1988, pp. 113-134.

8. S.E. Rogers & D. Kwak, "An Upwind Differencing Scheme for the Incompressible Navier-Stokes Equations", Appl. Numer. Math., Vol. 8, 1991, pp 43-64.

9. J. Kim and P. Moin, "Application of a Fractional-Step Method to Incompressible Navier-Stokes Equations", J. Comp. Phys., Vol. 59, 1985, pp. 308-323.

10. M.M. Rai and P. Moin, "Direct Simulations of Turbulent Flow Using Finite-Difference Schemes", AIAA-89-0369,1989.

11. H. Le and P. Moin, "An Improvement of Fractional-Step Methods for the Incompressible Navier-Stokes Equations", J. Comp. Phys., Vol. 92, No. 2, 1991, pp. 369-379.

12. C.J. Freitas, R.L. Street, A.N. Findikakis and J.R. Koseff, "Numerical Simulation of Three-Dimensional Flow in a Cavity," Inter. J. Numer. Meth. Fluids, Vol. 5, No. 6, 1985, pp. 561-576.

13. S.V. Patanka, Numerical Heat Transfer and Fluid Flow, Hemisphere, Washington, DC, 1980.

14. C.R. Maliska and G.D. Raithby, "A Method for Computing Three Dimensional Flows Using Non-Orthogonal Boundary-Fitted Coordinates," Inter. J. Numer. Meth. Fluids, Vol 4, 1984, pp. 519-537

15. G.E. Schneider and M. Zedan, "A Modified Semi-Implicit Procedure for the Numerical Solution of Field Problems," Numer. Heat Trans., Vol. 4, No. 1, 1981, pp.

16. S.A. Jordan and M.L. Spaulding, "A Fast Algorithm for Grid Generation," J. Comp. Phys., Vol. 104, No.1, 1993, pp. 118-128.

17. S.A. Jordan "An Iterative Scheme for Numerical Solution of Steady Incompressible Viscous Flows", Comp. Fluids, Vol. 21, No. 4, 1992, pp. 503-517.

18. M. Antonopoulos-Domis, " Large-Eddy Simulation of a Passive scalar in Isotropic Turbulence", J. Fluid Mech., Vol. 104, 1981, pp. 55-79.

19. H.S. Rhee, J.R. Koseff and R.L. Street, "Flow Visualization of a Recirculating Flow by Rheoscopic Liquid and Liquid Crystal Techniques," Exper. Fluids, Vol. 2, 1984, pp. 57-64.

20. J.R. Koseff and R.L. Street, "On End Wall Effects in a Lid-Driven Cavity Flow", J. Fluids Engr., Vol. 106, No. 1, 1984, pp. 385-389.

21. J.R. Koseff and R.L. Street, " The Lid-Driven Cavity Flow: A Synthesis of Qualitative and Quantitative Observations", J. Fluids Engr., Vol. 106, 1984, pp. 390-398.

22. U. Ghia, K.N. Ghia and C.T. Shin, "High-Re Solutions of Incompressible Flow Using the Navier-Stokes Equations and a Multigrid Method", J. Comp. Phys., Vol. 48, 1982, pp 387-411.

23. J.R. Koseff and R.L. Street, " Visualization Studies of a Shear Three-Dimensional Recirculating Flow, J. Fluids Engr., Vol. 106, No. 1, 1984, pp. 21-29.

24. G.I. Taylor, "Stability of Viscous Liquid Contained Between Two Rotating Cylinders", Phil. Trans. Roy. Soc. (London), Vol. 223, 1923, pp. 289-343.

25. H. Gortler, "On the Three-Dimensional Instability of Laminar Boundary Layers on Concave Walls," NACA Technical Memorandum, 1375, 1954.

26. S.W. Kim and T.J. Benson, "Comparison of the SMAC, PISO, and Iterative Time-Advancing Schemes for Unsteady Flows", Comp. Fluids, Vol. 21, No. 3, 1992, pp. 435-454.

DISTRIBUTION LIST

External

4521 ONR (Fein)
4523 ONR (Ng, Remmers, Voglesong)

Internal

Codes: 02244
0251
0261 (NLON Library)
0262 (NPT Library (2))
10
102 (Lima)
22
38
3891
411
80
81
821
83
832
8322 (Jordan (5))

Total: 25